Published in final edited form as:

Nat Methods. 2019 October ; 16(10): 1054–1062. doi:10.1038/s41592-019-0579-4.

Real-time volumetric microscopy of in-vivo dynamics and large-scale samples with SCAPE 2.0

Venkatakaushik Voleti[1,2], **Kripa B. Patel**[1,2,‡], **Wenze Li**[1,2,‡], **Citlali Perez Campos**[1,2], **Srinidhi Bharadwaj**[1,2], **Hang Yu**[1,2], **Caitlin Ford**[3], **Malte J. Casper**[1,2], **Richard Wenwei Yan**[1,2], **Wenxuan Liang**[1,2], **Chentao Wen**[4], **Koutarou D. Kimura**[4,5], **Kimara L. Targoff**[3], **Elizabeth M.C. Hillman**[1,2,6]

[1]Laboratory for Functional Optical Imaging, Department of Biomedical Engineering, Columbia University, New York, New York, USA

[2]Mortimer B. Zuckerman Mind Brain Behavior Institute, Columbia University, New York, New York, USA

[3]Department of Pediatrics, College of Physicians & Surgeons, Columbia University, New York, New York, USA

[4]Graduate School of Natural Sciences, Nagoya City University, Nagoya, Japan

[5]Center for Advanced Intelligence Project, RIKEN, Tokyo, Japan

[6]Department of Radiology, Columbia University Medical Center and New York-Presbyterian Hospital New York, New York, USA

Abstract

The limited per-pixel bandwidth of most microscopy methods requires compromises between field of view, sampling density and imaging speed. This limitation constrains studies involving complex motion or fast cellular signaling, and presents a major bottleneck for high-throughput structural imaging. Here, we combine high-speed intensified camera technology with a versatile, reconfigurable and dramatically improved Swept, Confocally Aligned Planar Excitation (SCAPE) microscope design that can achieve high-resolution volumetric imaging at over 300 volumes-per-second and over 1.2 GHz pixel rates. We demonstrate near-isotropic sampling in freely moving *C.*

*Corresponding Author: Hillman, Elizabeth MC (Elizabeth.hillman@columbia.edu).

‡Equal contributions

Author Contributions

V.V and E.M.C.H conceived of and designed the system. V.V., W.L.[1], K.B.P., C.P.C. and E.M.C.H constructed the system. H.Y. and W.L.[2] assisted and provided information for extended designs. V.V, W.L[1], K.B.P, C.P.C, S.B.S, R.W.Y and E.M.C.H performed the experiments. V.V, K.B.P, S.B.S, R.W.Y, M.J.C and E.M.C.H. analyzed data. C.F and K.T created the zebrafish lines and performed husbandry. C.W and K.K. developed the deep-learning tracking algorithm used for cardiomyocyte nuclear tracking and tracked the cells. V.V. and E.M.C.H. wrote and prepared the manuscript. All authors reviewed, edited and consulted on the manuscript text. [1]Wenze Li, [2]Wenxuan Liang.

Competing Financial Interests Statement

SCAPE intellectual property is licensed to Leica Microsystems for commercial development. VV, WL[1], KBP, CPC and EMCH have a potential financial conflict of interest relating to SCAPE microscopy.

Statistics and Reproducibility

See Statistics and Reproducibility section within Online Methods

elegans, and analyze real-time blood flow and calcium dynamics in the beating zebrafish heart. The same system also permits high-throughput structural imaging of mounted, intact, cleared and expanded samples. SCAPE 2.0's significantly lower photodamage compared to point-scanning techniques is also confirmed. Our results demonstrate that SCAPE 2.0 is a powerful, yet accessible imaging platform for myriad emerging high-speed dynamic and high-throughput volumetric microscopy applications.

Editor's summary

SCAPE 2.0 is a versatile imaging platform that enables real-time 3D microscopy of cellular function and dynamic motion in living organisms at over 100 volumes per second with minimal photodamage, and high-throughput structural imaging in fixed, cleared and expanded samples.

Introduction

The past two decades have seen dramatic improvements in techniques for molecular and genetic labelling of cellular function and structure in a wide array of model organisms [1–3]. However, imaging living samples in 3D 'at the speed of life' remains a significant challenge. Tissue clearing and expansion techniques are providing exquisite new views of cellular architecture and connectivity, but these large samples introduce significant imaging throughput challenges [4–6].

Most microscopy methods trade-off constraints on imaging speed, field-of-view, spatial resolution and sample geometry. As a result, samples requiring high-speed imaging over large 3D fields of view have simply been inaccessible, while researchers have to navigate an array of different microscope technologies to cover their laboratories' needs. It is also increasingly common to combine in-vivo or live-cell imaging with complex environments, chambers or behavioral rigs. These needs are at odds with the high cost and complexity of modern microscopes, which often necessitates their placement in shared core facilities where customization is a major challenge, or limits their use to affluent labs.

Swept confocally aligned planar excitation (SCAPE) microscopy[7] directly addresses many of these challenges. Our new SCAPE 2.0 design is a simple, reconfigurable and cost-effective platform that can provide depth-resolved, high speed imaging at over 100 volumes per second in diverse, intact or freely moving samples through a single, motionless objective lens. SCAPE's use of light-sheet illumination also provides significant phototoxicity and signal to noise benefits over point-scanning confocal microscopy, making it well-suited for high-speed, continuous imaging in-vivo and of sensitive samples [8–11]. The system's dramatically improved spatial resolution and large, uniform field of view introduces SCAPE 2.0 as a viable alternative to point-scanning and spinning disk confocal for 3D imaging applications where photobleaching is prohibitive, or for large samples where long imaging times have become a major bottleneck.

We demonstrate that SCAPE-2.0 can image dynamic neural activity in *C. elegans* worms with cellular resolution and with much reduced photobleaching compared to current approaches, and enables dual color 3D imaging of freely moving worms at speeds permitting

smooth tracking of cells. We demonstrate real-time 3D imaging of the beating heart of zebrafish embryos at over 300 volumes per second (VPS), enabling non-gated imaging of the 4D dynamics of blood flow, and analysis of beat-to-beat cardiac calcium dynamics. Finally, we demonstrate that the same SCAPE 2.0 system can be used for high-throughput structural imaging of large, intact samples including the flat-mounted mouse retina and cleared and expanded tissues. These diverse applications demonstrate the broad utility of SCAPE 2.0 for a wide range of different life-sciences applications.

1. Results

SCAPE 2.0 system design

When point-scanning microscopes are used for high-speed imaging, per-pixel integration times can become vanishingly short [11]. Light-sheet methods can overcome this limit because they image all of the pixels within an entire plane of the sample in parallel, increasing per-pixel integration times by orders of magnitude, while also dramatically reducing photodamage by selectively illuminating only the plane being imaged. However, the dual, orthogonal objective geometry of most light sheet systems limits their ability to image the kinds of intact or planar samples usually measured using point-scanning confocal and two-photon microscopy, while the need for separate excitation and detection scanning mechanisms physically restricts achievable volumetric imaging speeds.

SCAPE is a single-objective oblique light sheet approach, which achieves high-speed volumetric imaging by sweeping both its excitation sheet and co-aligned detection planes along the x-direction without requiring any sample or objective lens motion (Figure 1a) [7,11–15]. This geometry permits imaging of a wide range of intact and freely moving samples as illustrated in Figure 1b(i–iv) and c(iii).

Figure 1c shows SCAPE 2.0's optical layout and, along with Supplementary Note Figure 3, illustrates how fluorescence detected back through the primary objective lens (O1) creates a focused image of the y-z' oblique light sheet at an intermediate image plane using a second objective lens (O2). This intermediate oblique image is rotated via a third objective lens (O3) and focused onto a camera [16]. This optical rotation ensures that the camera's view is focused on the oblique (y-z') illuminated plane in the sample providing an optically-sectioned light sheet image. The detection NA and crossing angle between the light sheet and detection view is dependent on the collection efficiency of the image rotation between O2 and O3 [7,16], as discussed further in Supplementary Note 3.

For fast imaging of a 3D volume, SCAPE 2.0 uses a large-aperture galvanometer mirror positioned between the primary and secondary objective lens telescopes such that it is relayed onto the back focal plane of both objective lenses in a 4f-configuration. Scanning this galvanometer mirror moves the position of the oblique light sheet across the sample in the x-direction, with the angle of the light sheet with respect to the optical axis remaining constant over the sweep. This same galvanometer mirror also serves a critical second function - it de-scans the returning fluorescent light such that the intermediate image of the oblique light sheet remains stationary. As a result, the camera always maintains its focus on

the obliquely illuminated plane, even as the plane scans through different xn-y-z' planes of the sample.

The galvanometer scans a sawtooth function at the desired volume rate – e.g. 10Hz for 10 VPS imaging. A 3D image is formed by stacking sequential y-z' planes into a 3D volume – a step that requires no mathematical reconstruction except for correction for the oblique angle of the light sheet (skew-correction – see Supplementary Figure 1). The camera reads out only the number of rows needed to sample the depth (z') range of the sample, enabling much faster frame rates than full-chip read-out (in our examples, 1,000–18,000 oblique frames per second (FPS)). An image splitter positioned in front of the camera permits side by side dual color images to be acquired simultaneously without increasing the number of rows acquired, and thus without sacrificing imaging speed. Several laser beams can be combined to permit simultaneous or interlaced imaging of multiple fluorophores.

SCAPE 2.0's significantly improved performance compared to our first demonstration[7] was achieved through careful optimization of lenses, including using a Powell lens for more uniform light sheet formation[17], a Plössl scan lens to reduce aberrations such as field curvature, maximization of detection numerical aperture (NA), sample-dependent adjustment of the light sheet NA, use of optimized tube lenses at the camera and overall improved alignment procedures. The system's improved detection efficiency combined with a state-of-the-art intensified camera yielded an order of magnitude increase in volumetric imaging speeds (>100 VPS). Another key feature of SCAPE 2.0 is its ability to image a diverse array of samples at different objective orientations, resolutions, magnifications, 3D fields of view and speeds. All imaging examples shown here were acquired with the same basic optical layout between objectives O1 and O2. The only changes between configurations (defined in Supplementary Table 1) come from interchanging objective lens O3, the camera tube lens and the camera. 1c(ii) depicts this detection module in an alternative O3/tube/camera configuration, which can also include a commercial zoom lens for continually adjustable magnification. Simple switching of the camera and / or tube lens is facilitated by their vertical orientation, while our novel image splitter permits both dual-color imaging and fine adjustment of the image position on the camera. Since O1 and O2 are never altered, the angle of the intermediate image plane remains constant, such that most reconfigurations could be done during an experiment and require minimal system realignment. SCAPE 2.0's single, off the shelf galvanometer mirror, instead of SCAPE's original polygon mirror, greatly simplifies alignment, improves stability and enables faster scanning speeds and avoids the need for customized parts anywhere in the system. Supplementary Note SN3 provides SCAPE 2.0 parts lists, further details regarding selection and optimization of each component of the system, as well as a number of alternative system configurations.

For each demonstration shown below, the configuration of SCAPE 2.0 is defined in Supplementary Table 1. All sample preparation and data analysis details are provided in Online Methods, while full imaging parameters for every dataset are provided in Supplementary Table 2.

High-resolution and high-speed imaging of C. elegans

With a nervous system consisting of only 302 neurons, Caenorhabditis elegans roundworms' small size and relative simplicity makes them an ideal model organism in neuroscience research. Imaging of neural activity with fluorescent protein-based calcium indicators such as GCaMP[1], combined with a well-established connectome, can allow increasingly sophisticated modeling of neural circuits during complex behaviors.

The current state of the art for functional *C. elegans* imaging is spinning disk confocal, typically acquiring 30–40 depths within the worm's head over a 50 micron depth range at 6 VPS [18,19]. However, the duration of such recordings is limited by photobleaching, while 6 VPS imaging makes tracking cells a major computational challenge. Methods such as temporal focusing two-photon, light-field microscopy and dual-view inverted selective plane illumination microscopy (di-SPIM) light-sheet have yet to achieve the combined speed, field of view and resolution needed to capture the entire freely moving adult worm [20,21,22].

Imaging of neuronal activity throughout the worm brain

For *C. elegans* imaging, SCAPE 2.0's system magnification was increased, while its diffraction-limited resolution was improved by increasing both its detection NA and the light-sheet's NA (~26.66x, effective detection NA: 0.35, sheet width ~1.2–1.8 μm over a ~20–40 μm depth range). See Supplementary Note SN1 for bead-based resolution characterization and comparison of different SCAPE configurations.

To compare SCAPE 2.0 to spinning disk confocal microscopy studies [19], we used configuration Az (see Supplementary Table 1) to image the head of a tetramisole-immobilized young adult *C. elegans* worm expressing nuclear-localized GCaMP6s and tagRFP at 5.96 VPS for 10 minutes (Figure 2a and Supplementary Video 1, see Online Methods for sample details andSupplementary Table 2 for full imaging parameters). The worm was mounted in agar under a glass coverslip and imaged from above. Dual-color data were acquired at 477 FPS using a total of 0.14 mW of 488 nm and 516 nm light at the sample. These parameters provided 5–10x denser sampling in z compared to typical spinning disk sampling: (0.32 × 0.32 × 1–2 μm/voxel x-y-z versus SCAPE 2.0: 0.75 × 0.24 × 0.19 μm/voxel x-y-z). To account for slight drifts, 4D tracking of the tagRFP-labeled nuclei was used to extract red and green fluorescence signals from 113 individual neurons within the head. Figure 2c shows raw GCaMP signals extracted from each cell demonstrating exceptional signal to noise and photostability. Supplementary Figure 2 shows minimal variation in RFP signals compared to GCaMP6s ΔF/F0 signals[12].

In keeping with previous studies[23], neurons in the immobilized worm exhibited distinct patterns of calcium activity (Figure 2c), affording the chance to explore their dynamic "functional connectivity". Correlation matrices between cells, within a ~30 second temporal sliding-window, were repeatedly k-means clustered to yield six cluster medians[24] (Figure 2d) representing six different patterns of correlation that the nervous system appears to switch between (Figure 2e). Connectivity states 1 and 2 depict strong anti-correlations between subsets of neurons, while in states 5 and 6 over 50% of the neurons are highly

correlated. A repeated motif of switching between states 2–4-1–4-6–4 occurs twice during the 10-minute run.

Supplementary Note SN2 and Supplementary Video 2 compare spinning disk confocal microscopy and SCAPE 2.0 photobleaching rates in living *C. elegans* worms. Results show that for equivalent spatiotemporal sampling, SCAPE 2.0 can acquire 25x more volumes than spinning disk confocal before reaching similar levels of photobleaching. This phototoxicity benefit can be leveraged to achieve longer duration in-vivo recordings, higher imaging speeds, finer sampling densities and/or larger fields of view.

High-speed, high-resolution imaging of neurons in a freely moving worm

Supplementary Video 3 shows that SCAPE 2.0 in configuration A_z can be used to capture calcium activity in the head of an un-anesthetized *C. elegans* worm. However, a faster camera is needed to sample the whole body of a freely moving worm with a high enough sampling density to resolve single neurons, combined with a fast enough volume-rate to chart the trajectories of cells during natural movements.

The HiCAM Fluo intensified sCMOS camera (Lambert Instruments) can read-out its 1280 × 1024 pixel sensor at 1,000 FPS, and can read at 6,900 FPS over a reduced 1280 × 128 pixel ROI. Combining SCAPE 2.0 with the HiCAM camera (configuration A_H), permitted 25.75 VPS dual-color imaging of a freely moving nuclear GCaMP6s/tagRFP *C. elegans* worm constrained within a 392 × 299 × 41 μm arena with a 1.42 × 0.37 × 0.32 micron μm x-y-z sampling density. Figure 2f–g and Supplementary Video 6 demonstrate that trajectories of individual cellular nuclei can be tracked continuously in the freely moving animal. A larger field of view can be imaged at 10 VPS with single-color imaging, demonstrated in Supplementary Figure 3 and Supplementary Video 5 for a GFP-expressing worm in which cell bodies and dendritic processes can be clearly seen along the body wall.

Supplementary Video 6 shows a 3 minute long, 20 VPS dual-color SCAPE 2.0 dataset acquired on another freely moving GCaMP/RFP worm (configuration C_H). The video, and kymograph-based visualization of single-cell GCaMP activity in Supplementary Figure 4 reveals both fast (~1 second) and slower (~5–10 second) GCaMP transients in head neurons, as well as motion-related firing of body and tail neurons. The last two minutes of the video captures vigorous 3D motion of the animal. Supplementary Figure 5 shows results of semi-automated tracking using Imaris (Bitplane) of 22 head and 8 body neurons over a 2 minute period in another worm (see Online Methods for important analysis considerations). Although underscoring the need for more robust tracking and signal extraction algorithms, these results demonstrate that SCAPE 2.0 has both the temporal and spatial resolution for comprehensive extraction of neuronal signaling events throughout the entire freely moving worm. SCAPE's versatile imaging geometry can accommodate C. elegans within more complex microfluidic chambers, while its low phototoxicity should enable prolonged imaging during complex behaviors.

High speed imaging of the beating zebrafish heart

Studies of the embryonic zebrafish heart can provide insights into the way that the vertebrate heart develops, as well as the influence of genetic and environmental factors on structural

and functional cardiac development[25]. However, real-time imaging of the heart beating naturally at 2–4 Hz has been difficult to achieve. Time-gated light-sheet techniques that build up a volumetric image by acquiring each plane across many beats[26,27] require periodicity and so cannot capture irregular arrhythmias or permit fully 4D particle tracking for red blood cell (RBC) flow analysis [28]. Requiring >2 cardiac cycles per plane, time-gating can also need over 100 seconds of exposure to reconstruct a single 4D cardiac cycle. Real-time cardiac imaging using an electrically tunable lenses (ETL) to maintain the system's focus on a moving light sheet has been achieved, yet is challenging to synchronize at high speeds [10,29].

Ultra-high-speed, real-time SCAPE 2.0 imaging of blood flow the beating zebrafish heart:

Figure 3a–b shows SCAPE 2.0 imaging results obtained in 3 days post-fertilization (dpf) zebrafish embryos expressing GFP and DsRed in its endothelial cells and RBCs respectively [30,31]. The fish was positioned in a drop of agar on a glass-bottomed Petri dish and imaged from below. 100 VPS, dual-color images were acquired with SCAPE 2.0 in configuration B_H. The HiCAM camera captured a 640 × 148 pixel ROI (320 pixels per color) at 12,719 FPS, permitting 127 x-steps per volume and an effective sampling density of 1.41 × 1.07 × 0.86 μm (x-y-z). Despite this 1.21 GHz pixel rate, only 1 mW of 488 nm illumination was incident at the sample. Supplementary Video 8 shows both the heart's 3D motion, and RBC flow dynamics. Kymographs extracted from this data enable simple quantification of movements and blood flow patterns in the atrium and ventricle and their beat to beat relationship with the opening and closing of inflow, atrioventricular and outflow valves (Figure 3a.i–v).

Using a slightly smaller region of interest (ROI), HiCAM frame rates of 18,308 FPS permitted 321 VPS, dual-color cardiac imaging (Supplementary Video 9, Figure 3b.i). At this volume rate, travel of single RBCs through high-speed flow areas such as the atrioventricular canal during atrial systole could be tracked (see Methods). Figure 3b.ii–iii show an overlay of the full 3D trajectories of 16 cells traveling from the atrium to the ventricle at speeds of up to 3.8 mm/sec. Supplementary Figure 6 and Supplementary Figure 7 relate the speed of these cells to the cardiac cycle. Cells demonstrate a variety of behaviors including a typical transit through the AV canal, retrograde regurgitant flow during ventricular contraction, failure to pass into the ventricle during atrial contraction and staying for extended periods in the ventricle prior to passage through the bulbus arteriosus.

Ultra-high-speed SCAPE 2.0 imaging of calcium dynamics in the beating zebrafish heart:

100 VPS dual-color SCAPE 2.0 data was also acquired in 3-dpf zebrafish embryos expressing calcium-sensitive GCaMP and static DsRed in their myocardial cytosol and nuclei respectively [32,33]. Figure 3c shows a single raw volume acquired in 0.01 seconds. A deep-learning based cell segmentation and tracking algorithm [34] was used to track the DsRed cardiomyocyte nuclei as fiducials on the heart wall, with 67 cells reliably tracked over multiple beats (see Supplementary Video 10). Figure 3d depicts the speeds of each tracked cell's 3D movement during a cardiac cycle (between 0 and 0.6 mm/s). Fluorescence signals extracted from the tracked ROIs along each nucleus's trajectory exhibit periodic fluctuations for both Red (DsRed) and green (GCaMP) channels, due to the periodic

compression of cells, shadowing and tracking errors (Figure 3e.i). However, a green / red ratio (R) should cancel out these common effects, leaving only calcium-dependent fluorescence changes (see Online Methods for analysis details and exclusion criteria). Figure 3e.i and Supplementary Figure 8 shows ΔR/R exhibiting temporal shapes that are consistent with prior observations of calcium dynamics in both the atrium and ventricle [27]. Figure 3f depicts these metrics for two atrial and ventricular cells as a function of their paths during 9 repeated heartbeats.

To further confirm detection of calcium-dependent transients in the beating heart, imaging was repeated in the same fish after cardiac paralysis with 2,3-butanedione monoxime (BDM), a chemical electromechanical decoupler that ceases cardiac motion while maintaining calcium transients [35]. The accessibility of the fish during SCAPE imaging permitted drug administration with minimal disruption, such that identical cardiac cells could be identified before and after BDM application. Figure 3e.ii and Supplementary Figure 8 compare these cells' fluorescence dynamics when moving and stationary. Cell tracking confirmed minimal physical movement after BDM, while extracted DsRed signals are accordingly largely flat (see Supplementary Video 11). However, GCaMP signal dynamics, although substantially slower after BDM, remain consistent in their temporal shape with ratios extracted from the physically beating heart.

These results demonstrate SCAPE's capacity for comprehensive analysis of cardiac function, including development of the heart's conduction system in health and disease. SCAPE 2.0's ability to evaluate real-time responses to pharmacological interventions or other perturbations within the same living animal was also demonstrated. Such experiments are greatly facilitated by the short acquisition times needed to capture complete cardiac cycles using SCAPE, and the ability to avoid paralysis of the fish's heart during longitudinal imaging. Beyond biological samples, these examples also demonstrate SCAPE2.0's ability to perform 4D particle tracking and velocimetry, elastography and to extract complex fluid flows in diverse application areas.

Large field of view structural imaging with SCAPE 2.0 microscopy

Structural imaging of large samples with complex 3D structures, such as fixed, flat-mount retinas and organoids has become a major bottleneck for microscope facilities. The value of cleared and expanded tissues is truly unlocked when they are imaged in-toto, with sufficient isotropic resolution to resolve of the distribution, connectivity, molecular and genetic properties of cells[4,5]. Light-sheet systems optimized for imaging large, cleared samples face many trade-offs in terms of sampling density, achievable NAs, sample positioning and image stitching that restrict throughput [36]. Inverted-SPIM geometries can better accommodate planar samples, but face immersion media and sample translation challenges, and cannot leverage the full working distance of their objective lenses[37,38].

SCAPE 2.0 for rapid structural imaging of planar, fixed specimens

Figure 4a–d shows structural images of a fixed, uncleared, flat-mounted mouse retina imaged using SCAPE 2.0. The retina expressed GFP predominantly within the ganglion cells and Aii amacrine cells of the retina *(AAV2-CAG-ChR2-GFP-Na1.6)* [39].

High magnification retinal images in Figure 4b–d were acquired with SCAPE 2.0 in an upright configuration (Figure 1b(iii)) with 26.66x magnification and an effective detection NA: 0.35 (configuration Az). A field of view of approximately 700×500×75 μm was imaged permitting clear visualization of not only cell bodies, but also individual processes extending throughout the sample (see Supplementary Video 12 for a depth fly-through).

To capture images of the entire retina in Figure 4a and Supplementary Video 13, SCAPE 2.0 was configured to have ~4.66x magnification with effective detection NA: ~0.23 (configuration D_z). SCAPE 2.0 was used in an inverted configuration with the glass slide positioned coverslip down (with a drop of water for immersion) on a platform held by a 3-axis motorized translator (Figure c(iii)). Data was then acquired by keeping SCAPE's galvanometer mirror stationary, and moving the sample through the oblique sheet at constant velocity in a similar way to oblique plane microscopy (OPM) [16]. This approach permits imaging of x-y-z' volume-strips with almost indefinite x-direction extents (see 1b(iii–iv)) with x-sampling density governed by the camera frame rate relative to the translation speed. The whole retina was sampled in 128 seconds by acquiring 7 adjacent, overlapping volume-strips using a 680 × 275 pixel camera ROI (y-z' field of view of 930 × 313 μm) acquired at 250 FPS, while the x-stage was moved at 0.25 mm/second. These 7 volume strips were then stitched to generate a field of view of ~4.75 × 4.35 × 0.235 mm. The projections in Figure 4a demonstrate the near-uniform resolution and sampling density, as well as the rich, depth-resolved information available across the entire sample with minimal stitching artifacts. Cells are visible in the ganglion, inner nuclear layer and outer nuclear layers.

SCAPE 2.0 stage-scanning mode for rapid structural imaging of cleared brains

Figure 4e–g and Supplementary Video 14 show a stage-scanning SCAPE 2.0 image an mCUBIC[6,40] cleared Thy1-GFP mouse brain that was sliced coronally and imaged from below in a glass-bottomed Petri dish (configuration D_z, Figure 1b(iv) and c(iii)). 18 adjacent, overlapping volume strips, 1.10 mm wide in y and 456 microns deep were acquired with 1 micron x-spacing at 520 FPS and stitched and cropped into a ~8.37 × 9.06 × 0.385 mm volume with a sampling density of 1 × 1.37 × 1.14 μm x-y-z. Total acquisition took 242 seconds. Color depth-encoding demonstrates how SCAPE 2.0's near-uniform sampling enables clear tracing of axons and dendrites across large areas of the intact brain. Supplementary Figure 10 and Supplementary Video 15 and Supplementary Video 16 show results from this same cleared brain using 66.6x magnification (configuration G_z), enabling visualization of fine details of dendritic spines. In both cases, no compensation for the refractive index of mCUBIC tissues was used except for refocusing of objective O3.

Imaging deep into expansion microscopy samples using SCAPE 2.0

The examples above used low NA light sheets to span a depth range of up to ~450 microns. However, Figure 4h and Supplementary Figure 11 demonstrate SCAPE 2.0's ability to image almost 2 mm deep into a thick 4x expanded mouse spinal cord cross-section with ChAT-Tomato/Thy1-YFP expression by stitching z-overlapping, ~250 micron thick volume-strips, down to the limit of the primary objective lens' 2mm working distance. Imaging was performed in an inverted, stage-scanning configuration at two different magnifications (configurations D_z, ~4.66x and Ez, ~11.4x) collecting 2 × 1 × 1.8 mm and 0.5 × 1 × 1.73

mm (xyz) fields of view respectively. Total image acquisition times in both cases were around 100 seconds (9–11 volume strips each taking 4–5 seconds, +55 seconds for stage resetting time). Cell nuclei, continuous projections and spines are clearly resolved.

These results demonstrate SCAPE 2.0's capacity for high-throughput structural imaging, in addition to a high-speed functional microscopy. SCAPE 2.0 can accommodate slide-mounted fixed samples or specimens in dishes, while stage-scanning permits imaging of intact sample of almost unlimited x-y extent, while requiring far fewer stitching operations than systems that must tile 2D planes. SCAPE's single-objective geometry should enable access to the full working distance of modern high-NA long working distance objective lenses, a property that is especially valuable for expansion microscopy samples that can be very large, fragile and challenging to section [4], while faster imaging can overcome issues with sample swelling, motion and drift. We also note that the uniformity and extent of SCAPE 2.0's depth of field could be improved by adopting waist-scanning approaches [41] and adaptive optics to correct for sample-induced aberrations[42,43].

Discussion

Here, we demonstrated how SCAPE microscopy can meet diverse multi-scale imaging needs across the life sciences, including samples more usually assessed using point-scanning or spinning disk confocal microscopy, while delivering major advantages including reduced photobleaching and orders of magnitude faster volumetric imaging speeds. SCAPE 2.0's extraordinary speed enables tolerance of 3D motion, tracking of cellular movements in 3D space at high speeds, and quantification of dynamic changes in the fluorescence of functional indicators in 3D networks and structures. These imaging capabilities are responsive to the rapidly evolving set of fluorescent markers of cellular function, optical actuators of activity, and recognition that the 3D microenvironment of cells is a major factor that cannot be recapitulated in 2D cultures and isolated preparations.

We further demonstrated that SCAPE's simple and versatile single-objective imaging geometry provides opportunities for imaging large intact samples, well-plate, microfluidic and other high-throughput configurations as well as integration of SCAPE microscopy into experiments with complex behavioral components or environmentally controlled imaging. Importantly, in addition to these imaging performance advantages, this versatile, remarkably simple and easy to use SCAPE 2.0 implementation can be constructed using entirely off the shelf, affordable components. making it widely accessible to diverse researchers, including individual labs.

The simplicity of SCAPE's method of 3D image formation, low phototoxicity and versatile sample geometries mean that the approach can readily be extended to even broader, multi-scale imaging applications, where high-speed volumetric imaging would reveal new insights. This continued innovation and integration can leverage ever-improving cameras, objectives and fluorescent indicators for further performance improvements. Although SCAPE's high data rates are a strength, the very large datasets produced present new challenges for data storage, data sharing and holistic analysis. Improved approaches for information extraction, quantification and meaningful interpretation, possibly leveraging the rapidly maturing

capabilities of artificial intelligence, could streamline analysis and make SCAPE's rich data even more accessible to end users.

Supplementary Material

Refer to Web version on PubMed Central for supplementary material.

Acknowledgements

We would like to thank J. Herz from Lambert Instruments and P. Clemenceau from Axiom Optics for demonstrating and helping to support the HiCAM Fluo camera, and B. Witover from Morell Instruments for assistance with lens testing. *C. elegans* strains were provided by the Caenorhabditis Genetics Center (funded by NIH Office of Research Infrastructure Program No. P40OD010440). We sincerely thank D. Cosio and E. Boyden (MIT), O. Hobert and E. Yemini (Columbia), F. Randi and A. Leifer (Princeton) and R. Dunn and S. Kato (UCSF) for their help and advice with respect to *C. elegans* imaging. We thank C. de Sena Tomás (Columbia) for assistance in providing zebrafish embryos for heart studies. We thank T. Zheng, S. Huang and O. Gerard (Columbia) for their advice and assistance with TrackPy and *C. elegans* cell tracking and L. Hammond (Columbia) for help with spinning disk confocal photobleaching experiments. We thank B. Young and N. Tian (U of Utah) for providing the retinal flat mount sample and A. Narasimhan and P. Osten (Cold Spring Harbor) for providing the mCUBIC cleared mouse brain sample. We thank F. Shen and D. Cai (U of Michigan) for preparing the expanded spinal cord slice and G. Valdez (Virginia Tech) for providing the spinal cord tissue. We thank M. Bouchard for training and foundational work on SCAPE, other members of the Hillman lab and our collaborators including W. Grueber, D. Schoppik and R. Bruno for support and assistance on many aspects of this work.

Funding Sources

Funding for this work was provided by National Institutes of Health BRAIN initiative grants 5U01NS09429, UF1NS108213 (EMCH) and U19NS104649 (PI-Costa) and R01HL13143801A1 (KLT), the National Science Foundation NSF-GRFP DGE-1644869 (KBP), IGERT 0801530 (VV) and CAREER CBET-0954796 (EMCH), the Simons Foundation Collaboration on the Global Brain (542951, RA/LA/EMCH), Department of Defense MURI W911NF-12–1-0594 (RY/EMCH), the Kavli Institute for Brain Science and the Columbia-Coulter Translational Research Partnership and Coulter Foundation Early Career program (EMCH) and KAKENHI JP16H06545 by MEXT, Japan (to KK).

References

1. Chen TW. et al. Ultrasensitive fluorescent proteins for imaging neuronal activity. Nature 499, 295–300, doi:10.1038/nature12354 (2013). [PubMed: 23868258]
2. Tian L. et al. Imaging neural activity in worms, flies and mice with improved GCaMP calcium indicators. Nat Methods 6, 875–881, doi:10.1038/nmeth.1398 (2009). [PubMed: 19898485]
3. Boyden ES, Zhang F, Bamberg E, Nagel G & Deisseroth K. Millisecond-timescale, genetically targeted optical control of neural activity. Nat Neurosci 8, 1263–1268 (2005). [PubMed: 16116447]
4. Chen F, Tillberg PW & Boyden ES. Optical imaging. Expansion microscopy. Science 347, 543–548, doi:10.1126/science.1260088 (2015). [PubMed: 25592419]
5. Chung K & Deisseroth K. CLARITY for mapping the nervous system. Nat Methods 10, 508–513, doi:10.1038/nmeth.2481 (2013). [PubMed: 23722210]
6. Susaki EA. et al. Advanced CUBIC protocols for whole-brain and whole-body clearing and imaging. Nat Protoc 10, 1709–1727, doi:10.1038/nprot.2015.085 (2015). [PubMed: 26448360]
7. Bouchard MB. et al. Swept confocally-aligned planar excitation (SCAPE) microscopy for high speed volumetric imaging of behaving organisms. Nature photonics 9, 113–119, doi:10.1038/nphoton.2014.323 (2015). [PubMed: 25663846]
8. Tomer R. et al. SPED Light Sheet Microscopy: Fast Mapping of Biological System Structure and Function. Cell 163, 1796–1806, doi:10.1016/j.cell.2015.11.061 (2015). [PubMed: 26687363]
9. Ahrens MB, Orger MB, Robson DN, Li JM & Keller PJ. Whole-brain functional imaging at cellular resolution using light-sheet microscopy. Nat Methods 10, 413–420, doi:10.1038/nmeth.2434 (2013). [PubMed: 23524393]

10. Fahrbach FO, Voigt FF, Schmid B, Helmchen F & Huisken J. Rapid 3D light-sheet microscopy with a tunable lens. Optics Express 21, 21010–21010, doi:10.1364/OE.21.021010 (2013). [PubMed: 24103973]
11. Hillman EM. et al. High-speed 3D imaging of cellular activity in the brain using axially-extended beams and light sheets. Curr Opin Neurobiol 50, 190–200, doi:10.1016/j.conb.2018.03.007 (2018). [PubMed: 29642044]
12. Vaadia RD. et al. Characterization of Proprioceptive System Dynamics in Behaving Drosophila Larvae Using High-Speed Volumetric Microscopy. Current Biology 29, 935–+, doi:10.1016/j.cub.2019.01.060 (2019). [PubMed: 30853438]
13. Kumar M, Kishore S, Nasenbeny J, McLean DL & Kozorovitskiy Y. Integrated one- and two-photon scanned oblique plane illumination (SOPi) microscopy for rapid volumetric imaging. Opt Express 26, 13027–13041, doi:10.1364/OE.26.013027 (2018). [PubMed: 29801336]
14. Yang B. et al. Epi-illumination SPIM for volumetric imaging with high spatial-temporal resolution. Nat Methods 16, 501–504, doi:10.1038/s41592-019-0401-3 (2019). [PubMed: 31061492]
15. Zhang L, Capilla A, Song W, Mostoslavsky G & Yi J. Oblique scanning laser microscopy for simultaneously volumetric structural and molecular imaging using only one raster scan. Scientific Reports 7, 8591–8591, doi:10.1038/s41598-017-08822-0 (2017). [PubMed: 28819250]
16. Dunsby C. Optically sectioned imaging by oblique plane microscopy. Optics express 16, 20306–20316 (2008). [PubMed: 19065169]
17. Saghafi S, Becker K, Hahn C & Dodt H-U. 3D-ultramicroscopy utilizing aspheric optics. Journal of Biophotonics 7, 117–125, doi:10.1002/jbio.201300048 (2014). [PubMed: 23861302]
18. Venkatachalam V. et al. Pan-neuronal imaging in roaming Caenorhabditis elegans. Proc Natl Acad Sci U S A 113, E1082–1088, doi:10.1073/pnas.1507109113 (2016). [PubMed: 26711989]
19. Nguyen JP. et al. Whole-brain calcium imaging with cellular resolution in freely behaving Caenorhabditis elegans. Proc Natl Acad Sci U S A 113, E1074–1081, doi:10.1073/pnas.1507110112 (2016). [PubMed: 26712014]
20. Prevedel R. et al. Simultaneous whole-animal 3D imaging of neuronal activity using light-field microscopy. Nature Methods 11, 727–730, doi:10.1038/nmeth.2964 (2014). [PubMed: 24836920]
21. Schrodel T, Prevedel R, Aumayr K, Zimmer M & Vaziri A. Brain-wide 3D imaging of neuronal activity in Caenorhabditis elegans with sculpted light. Nat Methods 10, 1013–1020, doi:10.1038/nmeth.2637 (2013). [PubMed: 24013820]
22. Ardiel EL. et al. Visualizing Calcium Flux in Freely Moving Nematode Embryos. Biophys J 112, 1975–1983, doi:10.1016/j.bpj.2017.02.035 (2017). [PubMed: 28494967]
23. Kato S. et al. Global brain dynamics embed the motor command sequence of Caenorhabditis elegans. Cell 163, 656–669, doi:10.1016/j.cell.2015.09.034 (2015). [PubMed: 26478179]
24. Allen EA. et al. Tracking whole-brain connectivity dynamics in the resting state. Cereb Cortex 24, 663–676, doi:10.1093/cercor/bhs352 (2014). [PubMed: 23146964]
25. Weber M & Huisken J. In vivo imaging of cardiac development and function in zebrafish using light sheet microscopy. Swiss Med Wkly 145, doi:10.4414/smw.2015.14227 (2015).
26. Taylor JM. Optically gated beating-heart imaging. Front Physiol 5, 481, doi:10.3389/fphys.2014.00481 (2014). [PubMed: 25566083]
27. Weber M. et al. Cell-accurate optical mapping across the entire developing heart. Elife 6, 1–23, doi:10.7554/eLife.28307 (2017).
28. Zickus V & Taylor JM. 3D + time blood flow mapping using SPIM-microPIV in the developing zebrafish heart. Biomed Opt Express 9, 2418–2435, doi:10.1364/BOE.9.002418 (2018). [PubMed: 29760998]
29. Mickoleit M. et al. High-resolution reconstruction of the beating zebrafish heart. Nature Methods 11, 919–924, doi:10.1038/nmeth.3037 (2014). [PubMed: 25042787]
30. Beis D. et al. Genetic and cellular analyses of zebrafish atrioventricular cushion and valve development. Development 132, 4193–4204, doi:10.1242/dev.01970 (2005). [PubMed: 16107477]
31. Traver D. et al. Transplantation and in vivo imaging of multilineage engraftment in zebrafish bloodless mutants. Nat Immunol 4, 1238–1246, doi:10.1038/ni1007 (2003). [PubMed: 14608381]

32. Arnaout R. et al. Zebrafish model for human long QT syndrome. Proc Natl Acad Sci U S A 104, 11316–11321, doi:10.1073/pnas.0702724104 (2007). [PubMed: 17592134]
33. Mably JD, Burns CG, Chen J-N, Fishman MC & Mohideen M-APK. heart of glass Regulates the Concentric Growth of the Heart in Zebrafish. Current Biology 13, 2138–2147, doi:10.1016/j.cub.2003.11.055 (2003). [PubMed: 14680629]
34. Wen C. et al. Deep-learning-based flexible pipeline for segmenting and tracking in 3D image time series for whole brain imaging. BioArxiv, doi:10.1101/385567 (2018).
35. Kirchmaier BC. et al. The Popeye domain containing 2 (popdc2) gene in zebrafish is required for heart and skeletal muscle development. Dev Biol 363, 438–450, doi:10.1016/j.ydbio.2012.01.015 (2012). [PubMed: 22290329]
36. Hillman EMC, Voleti V, Li W & Yu H. Light Sheet Microscopy in Neuroscience. Annual Reviews Neuroscience (2019).
37. Glaser AK. et al. Light-sheet microscopy for slide-free non-destructive pathology of large clinical specimens. Nature Biomedical Engineering 1, s41551–41017, doi:10.1038/s41551-017-0084 (2017).
38. Glaser AK. et al. Multi-immersion open-top light-sheet microscope for high-throughput imaging of cleared tissues. bioRxiv (2019).
39. Wu C, Ivanova E, Cui J, Lu Q & Pan ZH. Action potential generation at an axon initial segment-like process in the axonless retinal AII amacrine cell. J Neurosci 31, 14654–14659, doi:10.1523/JNEUROSCI.1861-11.2011 (2011). [PubMed: 21994381]
40. Narasimhan A, Venkataraju KU, Mizrachi J, Albeanu DF & Osten P. Oblique light-sheet tomography: fast and high resolution volumetric imaging of mouse brains. bioRxiv, 132423, doi:10.1101/132423 (2017).
41. Dean KM, Roudot P, Welf ES, Danuser G & Fiolka R. Deconvolution-free Subcellular Imaging with Axially Swept Light Sheet Microscopy. Biophys J 108, 2807–2815, doi:10.1016/j.bpj.2015.05.013 (2015). [PubMed: 26083920]
42. Wilding D, Pozzi P, Soloviev O, Vdovin G & Verhaegen M. Adaptive illumination based on direct wavefront sensing in a light-sheet fluorescence microscope. Opt Express 24, 24896–24906, doi:10.1364/OE.24.024896 (2016). [PubMed: 27828430]
43. Garbellotto C & Taylor JM. Multi-purpose SLM-light-sheet microscope. Biomed Opt Express 9, 5419–5436, doi:10.1364/BOE.9.005419 (2018). [PubMed: 30460137]

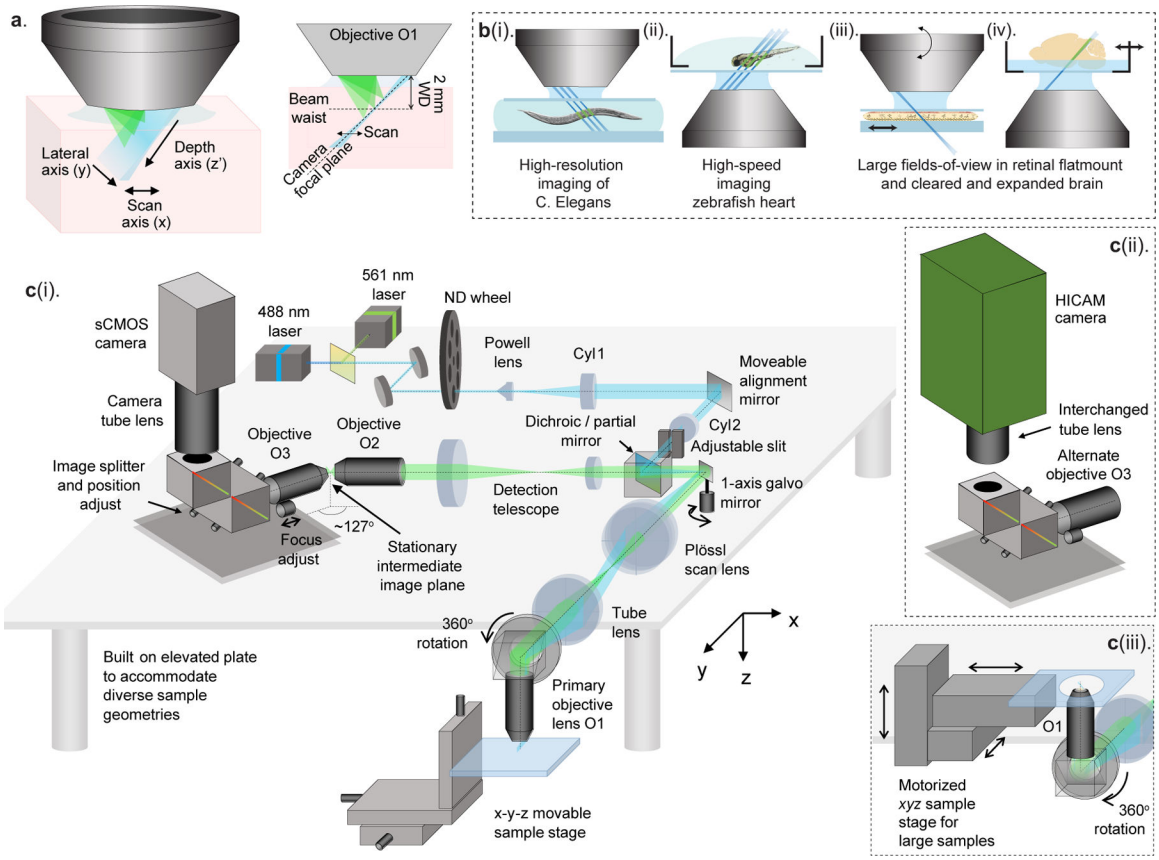

Figure 1. SCAPE 2.0 system configuration and sample geometries.

a. The SCAPE imaging geometry at the sample – an oblique light sheet illuminates the sample along y-z', while fluorescence light generated is detected back through the same objective lens. Galvanometer mirror scanning translates both the light sheet and detection plane along x. **b.** Experimental imaging configurations used in demonstrations provided in this paper. *C. elegans* (i) were imaged upright through a glass coverslip, zebrafish heart (ii), cleared and expanded brain (iv) were imaged in an inverted configuration through a glass bottom petri dish. Flat-mounted retina samples (iii) were imaged both upright and inverted. **c.** Schematic showing the layout of SCAPE 2.0. See Supplementary Note Figure 3 for a system photograph and optical layout, photos of different sample geometries and Supplementary Note Table 2 for a complete parts list. The system's adjustable slit modifies the light sheet NA, while fine-focus is adjusted at O3. (ii) The interchangeable components of the detection module (O3, camera tube / zoom lens and camera) enable widely varying magnifications and fields of view with no other changes to the basic layout. c(ii) depicts the system's rotating primary objective lens O1 in an inverted geometry, along with interchangeable motorized x-y-z stages for large sample positioning.

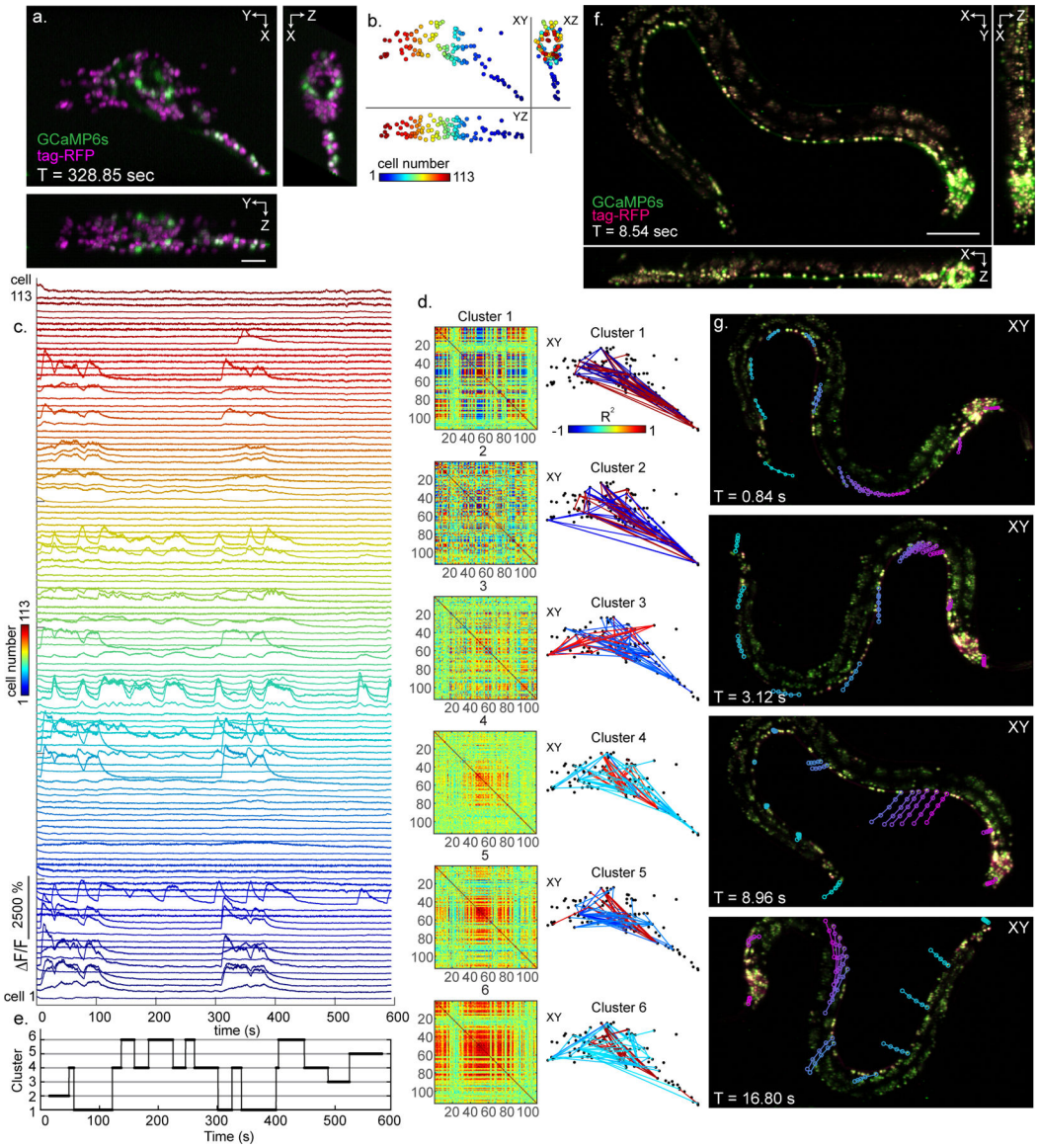

Figure 2. High resolution and high-speed SCAPE 2.0 imaging of *C. elegans* worms.

a. A single volume of SCAPE 2.0 data acquired at 5.96 VPS on the head of a living, immobilized *C. elegans* worm (NLS-GCaMP6s/tagRFP (AML32)), shown as top-down and side-facing maximum intensity projections (MIP) (see Supplementary Video 1 for full run), scale bar 10 μm, (configuration A_Z). **b.** 113 neurons were identified and tracked in 3D space over ~10 minutes and are here ordered and color-encoded along the rostral-caudal axis. **c.** Extracted raw GCaMP6s fluorescence time-courses extracted from all of these tracked cells over 10 minutes. **d.** The 113 time-courses were correlated to each other over a 30 second moving window, and clustering of these correlation maps yielded the 6 cluster medians shown on the left, representing the most common states of correlated activity between the cells (see Online Methods). The graphs shown to the right illustrate the connections between the 50 highest and lowest correlations in the adjacent cluster medians with nodes representing individual cells and colors of edges representing strength of correlations (on the

X-Y view of the worm). **e.** Dominant cluster medians at any given point in time vary over the course of the ~ 10 minute experiment demonstrating repeated motifs. **f.** Multi-view MIPs of a single volume acquired in a freely moving *C. elegans* worm using SCAPE 2.0 with the HiCAM camera (configuration A_H) at 25.75 VPS over a 392 × 299 × 41 μm field of view with 1.42 × 0.37 × 0.32 micron sampling (x-y-z). Scale bar 50 μm. **g.** X-Y MIPs of different volumes showing cell positions tracked in the preceding 5 time points (total 0.19 sec) (see Supplementary Video 4 and additional worms, analysis and tracking in Supplementary Video 6 and Supplementary Video 7 and Supplementary Figure 4 and Supplementary Figure 5).

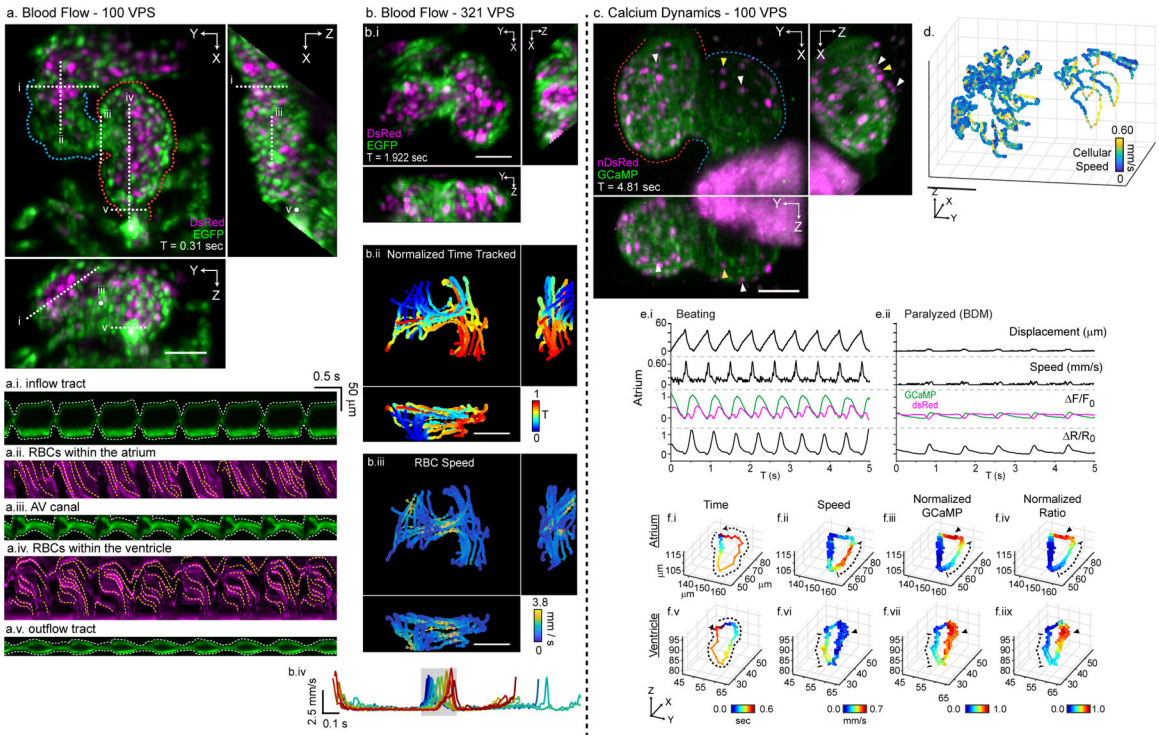

Figure 3. Real-time high-speed SCAPE 2.0 imaging of the zebrafish heart

a-b. Imaging blood flow in the embryonic zebrafish heart using SCAPE 2.0 with the HiCAM camera (configuration BH). EGFP labels endothelial cells (green), while DsRed (magenta) labels red blood cells (RBCs) (*Tg(flk1:EGFP)*^{s843}*; Tg(gata1:DsRed)*^{sd2}) **a.** MIP of a single volume in the zebrafish heart acquired at 100 VPS. Atrial and ventricular outlines are shown in blue and red respectively. (Full Video in Supplementary Video 8) **a.i-v.** Kymographs taken along the white dashed lines shown in (a) **b.i.** MIPs of a single volume in the zebrafish heart acquired at 321 VPS. (Full Video in Supplementary Video 9) **b.ii.** Trajectories of 16 RBCs' motion through the heart with colors encoding the relative time of RBC's position along its trajectory from the atrium (blue) to the ventricle (red) **b.iii.** Same trajectories color-coded as RBC speed. **b.iv.** plots of these speeds, where the gray box indicates the duration of atrial contraction **c.** MIPs of a single volume acquired at 100 VPS on an embryonic zebrafish heart expressing calcium-dependent GCaMP (green) in the cardiomyocyte cytosol, and DsRed (magenta) in its cardiomyocyte nuclei (*tg(myl7:GCaMP)*^{s878}*; Tg(−5.1myl7:nDsRed2)*^{f2}). Blue and red outlines indicate atrium and ventricle respectively. Cardiomyocyte nuclei locations were tracked in 3D over time using a deep-learning based cell segmentation and tracking algorithm (full videos beating / paralyzed heart with tracked cells are shown in Supplementary Video 10 and Supplementary Video 11). **d.** 3D visualization of the speed of successfully tracked nuclei in the beating heart during a 0.60 second window. **e.** Plots of the extracted displacement, speed, $\Delta F/F_0$ of the GCaMP and nDsRed signals, and the $\Delta R/R_0$ of the ratio between the GCaMP and dsRd signals for a single atrial cell indicated by the yellow arrow in (c) before (e.i) and after (e.ii) the application of electromechanical decoupler BDM. **f.** Trajectory of the atrial cell indicated by white arrow in over a 5 second interval (9 consecutive heartbeats) (c) with color encoding: (f.i) the time from start of the acquisition (arrows indicate the direction of travel)

(f.ii) the cell's instantaneous speed (dashed intervals indicate high-velocity portions), (f.iii) the $\Delta F/F_0$ of the cell's GCaMP signal normalized to its maximum, (f.iv) the $\Delta R/R_0$ of the cell's ratio-ed GCaMP/nDsRed ratiometric signal normalized to its maximum (arrows indicate time of highest calcium signal). **f.v-iix.** Trajectories of the ventricular cell indicated by the white arrow in (c) with color encoding the same metrics as in (f.i-iv). All scale bars are 50 μm.

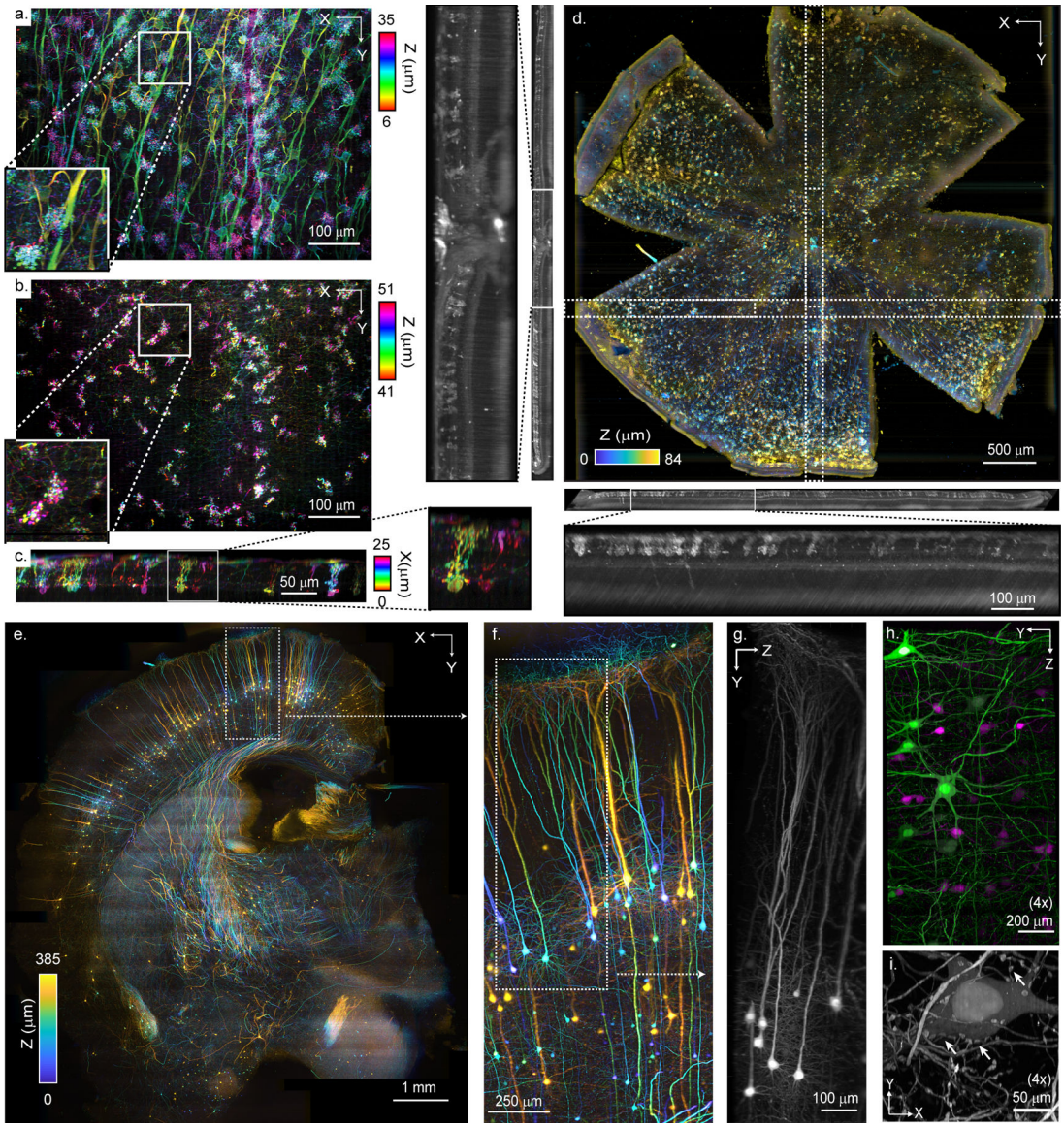

Figure 4. High throughput, large field of view structural imaging with SCAPE 2.0>

a-b. High-magnification imaging of an uncleared, fixed, stained mouse retinal flatmount shown as a top-down (XY) view in which colors encode depth over two different depth ranges. **c.** A side-view (YZ) of the same volume in which colors encode the x-position over a 25 μm range. The full extent of the Aii amacrine cells can be seen throughout the inner plexiform layer. Insets are zoomed by 2x. **d.** (Right) Color-depth (sub-range) encoded top-down view of the entire same mouse retinal flatmount acquired via stage-scanning and stitching. Insets left and below show side-view projections along the X and Y dimensions of regions indicated over the 235 μm thickness of the sample with insets showing the same dataset on a 4x larger scale. Supplementary Figure 9 compares the same region with high (**a**) and lower (**d**) magnifications. **e.** Color-depth encoded top-down view of a 385 μm thick volume acquired on a coronal hemi-section of an mCUBIC-cleared Thy1-GFP brain using stage-scanning and stitching. Scale bar 1mm. **f.** Zoomed view of subregion outlined in (**e**). **g.**

YZ MIP taken along the X direction of the subregion outlined in (**f**) demonstrating SCAPE 2.0's near isotropic sampling and resolution. **h-i.** Data acquired in a 4x expanded mouse spinal cord section. **h**. Dual-color data stitched along z-dimension over a 2 mm depth range, shown as an MIP over 1000 x-direction planes (1 mm). **i**. Zoomed in region from a higher magnification single-color dataset acquired on the same sample as a top-down MIP over 100 z-slices (45 μm). Arrows indicate detailed spine shapes. See Supplementary Figure 11 for full renderings of these datasets. To reduce dynamic range between bright soma and dimmer processes, **a, c, e-g**. are shown on a square root color scale whereas **b**. is shown on a quartic root color scale.